Structures in high-energy fusion data

H. Esbensen
Physics Division, Argonne National Laboratory, Argonne, Illinois 60439, USA
(Received 23 May 2012; published 13 June 2012)

Structures observed in heavy-ion fusion cross sections at energies above the Coulomb barrier are interpreted as caused by the penetration of centrifugal barriers that are well separated in energy. The structures are most pronounced in the fusion of lighter, symmetric systems, where the separation in energy between successive angular momentum barriers is relatively large. It is shown that the structures or peaks can be revealed by plotting the first derivative of the energy weighted cross section. It is also shown how an orbital angular momentum can be assign to the observed peaks by comparing to coupled-channels calculations. This is illustrated by analyzing high-energy fusion data for $^{12}C+{}^{16}O$ and $^{16}O+{}^{16}O$, and the possibility of observing similar structures in the fusion of heavier systems is discussed.

DOI: 10.1103/PhysRevC.85.064611 PACS number(s): 24.10.Eq, 25.70.Jj, 25.60.Pj

I. INTRODUCTION

The cross sections for the fusion of light, symmetric systems of nuclei sometimes exhibit structures or oscillations at energies above the Coulomb barrier. This has been observed both in measurements and in coupled-channels calculations. The best experimental examples of this behavior are the fusion data of $^{12}C+{}^{12}C$ [1] $^{12}C+{}^{16}O$ [2], and $^{16}O+{}^{16}O$ [3–5]. The structures have been associated with resonances but there are also suggestions that they may be caused by the penetration of centrifugal barriers that are well separated in energy [6,7].

A simple reason the oscillations occur primarily in the fusion of lighter, symmetric systems is that the separation in energy between successive angular momentum barriers is relatively large in these systems. Thus, when the separation of successive barriers becomes larger than twice the width associated with the penetration of the individual barriers, the oscillating pattern may occur. This feature will be illustrated by applying a simple model that is based on the Hill-Wheeler barrier penetration formula [8].

It was recently shown [7] that the structures observed in the $^{16}O+{}^{16}O$ fusion data of Ref. [4] can be explained fairly well by coupled-channels calculations. The calculations were based on a shallow potential in the entrance channel, whereas calculations based on a conventional Woods-Saxon potential did not reproduce the data so well [7]. Thus there appears to be some connection between the oscillations in fusion cross sections at energies above the Coulomb barrier and the fusion hindrance phenomenon that occurs at deep sub-barrier energies [9,10]. Both phenomena can be explained by applying a shallow M3Y + repulsion potential in coupled-channels calculations, whereas a conventional Woods-Saxon potential fails [7,11].

A model of heavy-ion fusion which contains information about the centrifugal barriers at high energies is introduced in the next section. It is based on the Hill-Wheeler formula for barrier penetration [8], and it is shown how the first derivative of the energy-weighted fusion cross section can be used as a diagnostic tool to reveal the heights of the centrifugal barriers. It is also shown why information about centrifugal barriers is lost in the commonly used Wong's formula [12]. In Sec. III, the first derivative of the energy-weighted cross section is applied to analyze the structures that are observed in the fusion data of $^{12}C+{}^{12}C$, $^{16}O+{}^{16}O$, and $^{12}C+{}^{16}O$. The possibility of observing similar structures in the fusion of heavier systems is discussed in Sec. IV, and Sec. V contains the conclusions.

II. MODEL BASED ON THE HILL-WHEELER APPROXIMATION

In order to make a simple interpretation of high-energy fusion data one may resort to the well-known Hill-Wheeler formula [8], which expresses the barrier penetration probability in terms of a simple Fermi function,

$$P_{\rm HW}(x) = \frac{\exp(x)}{1+\exp(x)}, \tag{1}$$

where $x = \big(E - V_B(L)\big)/\epsilon_0$. Here E is the center-of-mass energy, V_B is the barrier height, and ϵ_0 is a parameter that determines the exponential falloff at energies far below the barrier. The latter parameter can be derived from a parabolic approximation to the barrier potential but it is treated as an adjustable parameter in the following.

The fusion cross section can now be obtained from the expression

$$\sigma_f = \frac{\pi\hbar^2}{2\mu E}\sum_{L=0}^{L_{\rm max}}(2L+1)\,\frac{\exp(x_L)}{1+\exp(x_L)}, \tag{2}$$

where $x_L = \big(E - V_B(L)\big)/\epsilon_L$, and μ is the reduced mass of the fusing system. For a symmetric system of 0^+ ground state nuclei, the sum over angular momenta in Eq. (2) is restricted to even values of L and the cross section must then be multiplied by a factor of 2. There are two types of parameters in Eq. (2), namely, the L-dependent barrier heights, $V_B(L)$, and the decay constants ϵ_L.

The first derivative of the energy-weighted cross section obtained from Eq. (2) is

$$\left(\frac{d(E\sigma_f)}{dE}\right)_{HW} = \frac{\pi\hbar^2}{2\mu}\sum_{L=0}^{L_{\rm max}}(2L+1)\,\frac{1}{\epsilon_L}\,\frac{\exp(x_L)}{\big(1+\exp(x_L)\big)^2}. \tag{3}$$

This expression can be interpreted as a sum of individual L-dependent barrier distributions weighted with the factor $(2L+1)$. Each distribution is centered at the barrier height $V_B(L)$, and it has a width that is determined by the constant ϵ_L. The constants ϵ_L are assumed in the following to be independent of L, i.e., $\epsilon_L = \epsilon_0$.

A. Wong's formula

The model (2) was applied by Wong [12] to derive his formula for the fusion cross section. He assumed that the L-dependent barriers were parametrized as follows:

$$V_B(L) = V_{CB} + \frac{\hbar^2 L(L+1)}{2\mu R_{CB}^2}, \tag{4}$$

where V_{CB} is the height of the Coulomb barrier (for $L=0$), μ is the reduced mass of the system, and R_{CB} is the radial distance at the Coulomb barrier. By replacing the discrete sum over L in Eq. (2) with a continuous integration over L, i.e., $\sum_L (2L+1) \rightarrow \int d[L(L+1)]$, Wong obtained the following compact formula [12]:

$$\sigma_f = \pi R_{CB}^2 \frac{\epsilon_0}{E} \ln(1+\exp(x_0)), \tag{5}$$

where $x_0 = (E - V_{CB})/\epsilon_0$. The first derivative of Wong's formula,

$$\left(\frac{d(E\sigma_f)}{dE}\right)_W = \pi R_{CB}^2 \frac{\exp(x_0)}{1+\exp(x_0)}, \tag{6}$$

is proportional to a Fermi function and it approaches the value πR_{CB}^2 at energies far above the Coulomb barrier.

The barrier distribution for heavy-ion fusion reactions that was introduced in Ref. [13] is defined as the second derivative of the energy weighted cross section,

$$B(E) = \frac{d^2(E\sigma_f)}{dE^2}. \tag{7}$$

This definition was partly inspired by Wong's formula because the second derivative one obtains in this case,

$$\left(\frac{d^2(E\sigma_f)}{dE^2}\right)_W = \pi R_{CB}^2 \frac{1}{\epsilon_0} \frac{\exp(x_0)}{[1+\exp(x_0)]^2}, \tag{8}$$

is a nice symmetric distribution that is centered at the Coulomb barrier V_{CB} (for $L=0$.) The width is determined by ϵ_0, which characterizes the exponential falloff of the barrier penetrability at energies far below the s-wave barrier.

The definition Eq. (7) is reasonable at energies close to the Coulomb barrier. However, it does not reveal any information about the individual L-dependent barriers. A better way to search for evidence of the individual centrifugal barriers is to plot the first derivative of the energy weighted cross sections, according to the Hill-Wheeler expression, Eq. (3).

In order to be able to identify the individual centrifugal barriers from the measured fusion cross sections, it is necessary that the energy difference between successive barriers is much larger than twice the width of the individual barriers. Using the simple expression, Eq. (4), one obtains the following expression for the energy difference between the heights of successive barriers:

$$\Delta V_B = V_B(L+1) - V_B(L) \approx \frac{\hbar^2 2(L+1)}{2\mu R_{CB}^2}. \tag{9}$$

The width of the individual barrier distributions that appear in Eq. (3) is characterized by the parameter ϵ_L, which is assumed to be independent of L and equal to ϵ_0. The requirement that the energy difference, Eq. (9), is much larger than $2\epsilon_0$ implies that

$$(L+1) \gg \frac{2\mu R_{CB}^2 \epsilon_0}{\hbar^2}. \tag{10}$$

This condition applies to the fusion of an asymmetric system, where the fusion can occur for all values of L. For a symmetric system of 0^+ ground state nuclei, the fusion can only take place for even values of the angular momentum. The condition for observing individual barriers is then replaced by

$$(2L+3) \gg \frac{2\mu R_{CB}^2 \epsilon_0}{\hbar^2}. \tag{11}$$

B. Illustration of Hill-Wheeler's formula

Measured cross sections for the fusion of $^{16}\mathrm{O} + ^{16}\mathrm{O}$ [4,14] are compared in Fig. 1 to the Hill-Wheeler cross section (HW), Eq. (2), using the parameters $V_{CB} = 9.9$ MeV, $\epsilon_0 = 0.4$ MeV, and $R_{CB} = 8.4$ fm. These parameters provide a fair representation of the data above 8 MeV and are used below for illustrative purposes. Also shown is the coupled-channels calculation of Ref. [7] (solid curve) that is discussed in more detail in the next sections.

The first derivative of the energy-weighted cross section for the fusion of $^{16}\mathrm{O} + ^{16}\mathrm{O}$ is illustrated in Fig. 2. in terms of Wong's and Hill-Wheeler's formulas. The parameters used here are the same as those mentioned above. The first derivative of Wong's formula is a Fermi function which approaches the constant value πR_{CB}^2 at energies far above the Coulomb barrier, c.f. Eq. (6). The Hill-Wheeler expression, Eq. (3),

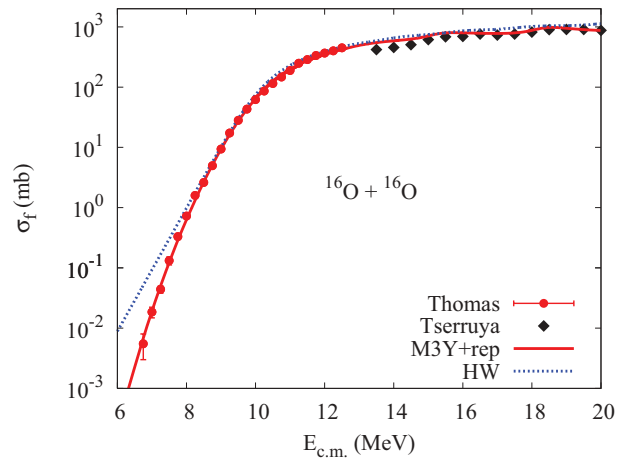

FIG. 1. (Color online) Measured cross sections for the fusion of $^{16}\mathrm{O} + ^{16}\mathrm{O}$ [4,14] are compared to the simplified Hill-Wheeler model (HW) with the parameters $V_{CB} = 9.9$ MeV, $R_{CB} = 8.4$ fm, $\epsilon_0 = 0.4$ MeV. The solid curve (M3Y + rep) is the result of the coupled-channels calculation presented in Ref. [7].

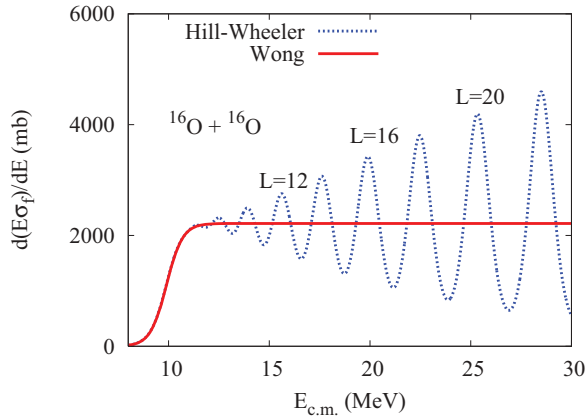

FIG. 2. (Color online) First derivative of the energy-weighted fusion cross sections for $^{16}O + ^{16}O$ obtained from Hill-Wheeler's and Wong's formulas. The parameters are the same as in Fig. 1. The expression obtained from Wong's formula, Eq. (6), behaves like a Fermi function and approaches πR_{CB}^2 at high energy. The Hill-Wheeler expression, Eq. (3), has the same behavior in the vicinity of the Coulomb barrier but starts to oscillate at high energies. The peaks show the location of the individual centrifugal barriers; the barriers for $L = 12$, 16, and 20 are indicated.

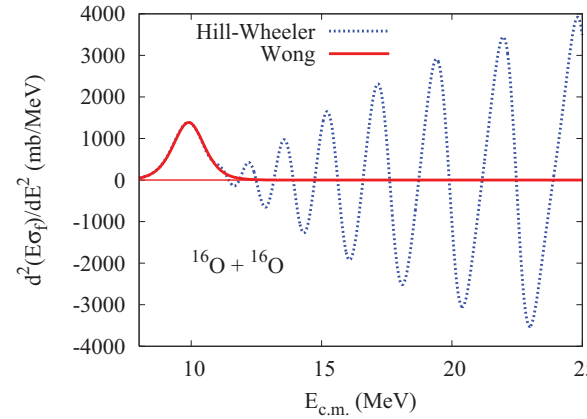

FIG. 3. (Color online) Second derivative of the energy-weighted fusion cross sections for $^{16}O + ^{16}O$ obtained from Hill-Wheeler's formula, Eq. (2), and from Wong's formula, Eq. (5). The parameters for the two expressions are quoted in the caption of Fig. 1. They produce almost identical results in the vicinity of the Coulomb barrier ($V_{CB} = 9.9$ MeV). The second derivative of Wong's formula goes to zero at high energies, whereas the Hill-Wheeler expression starts to oscillate.

reproduces this behavior at energies near and below the Coulomb barrier but it starts to oscillate at energies above the Coulomb barrier. The peaks in this figure reflect the location of the individual centrifugal barriers, as evidenced by Eq. (3). The peaks for $L = 12$, 16, and 20 are labeled in the figure.

The lowest peak that is visible in Fig. (6) is due to the centrifugal barrier for $L = 8$. This observation is consistent with the condition, Eq. (11), which in the example considered here requires that $(2L + 3) \gg 11$. The condition is not fulfilled for $L = 4$ or 6, but it is reasonably well satisfied for $L = 8$. As the angular momentum increases, the overlap between neighboring peaks diminishes which results in the breakdown of Wong's formula. The breakdown of Wong's formula is primarily a problem in light, symmetric systems, whereas it is usually not recognized in the fusion of heavy systems.

Let us for completeness also examine the conventional barrier distribution [13], i. e., the second derivative of the energy weighted cross section. The results one obtains in the example considered in this subsection are shown in Fig. 3. Wong's formula gives a symmetric distribution, Eq. (8), which is peaked at the Coulomb barrier. The distribution derived from Hill-Wheeler's formula reproduces Wong's formula in the vicinity of the Coulomb barrier but it starts to oscillate at higher energies. This illustrates vividly the breakdown of Wong's formula. It should be emphasized that the peaks in Fig. 3 at high energies do not represent the actual centrifugal barrier distributions; the barrier distributions at high energy are depicted in Fig. 2. It is only the peak at the lowest energy in Fig. 3 that represents a real barrier distribution, and it is associated with the angular momentum $L = 0$.

III. STRUCTURES IN LIGHT-ION FUSION

In this section the high-energy fusion data for $^{12}C + ^{12}C$ [1], $^{12}C + ^{16}O$ [2], and $^{16}O + ^{16}O$ [4] are compared to simple estimates based on the Hill-Wheeler formula and to coupled-channels calculations. The comparison is made in terms of the first derivative of the energy weighted cross section, which in the following is defined in terms of the average, finite difference value,

$$\left(\frac{d(E\sigma)}{dE}\right)_n = \frac{1}{2}\left[\frac{(E\sigma)_{n+1} - (E\sigma)_n}{E_{n+1} - E_n} + \frac{(E\sigma)_n - (E\sigma)_{n-1}}{E_n - E_{n-1}}\right]. \tag{12}$$

This definition is used to determine both the calculated and measured values. The energies E_n are the discrete energies where the measurements/calculations are performed. The average energy associated with the definition (12) is $\bar{E}_n = (E_{n-1} + 2E_n + E_{n+1})/4$.

The coupled-channels calculations are performed in the rotating frame approximation with ingoing-wave boundary conditions (IWBC) that are imposed at the minimum of the pocked of the entrance channel potential [11]. The fusion cross section is obtained from the ingoing flux at the boundary. A slight improvement is to impose the IWBC for each orbital angular momentum L at the minimum of the pocket in each centrifugal potential. This definition works quite well at energies near and below the Coulomb barrier but it can be difficult to account for the data at high energy. The problem can be solved by introducing an imaginary potential [11],

$$W(r) = \frac{W_0}{1 + \exp\big((r - R_w)/a_w\big)}, \tag{13}$$

where the radius parameter R_w is chosen to coincide with the location of the pocket minimum. At low energies, it is sufficient to use a weak and short ranged potential, with typical parameters $W_0 = -2$ MeV and $a_w = 0.2$ fm.

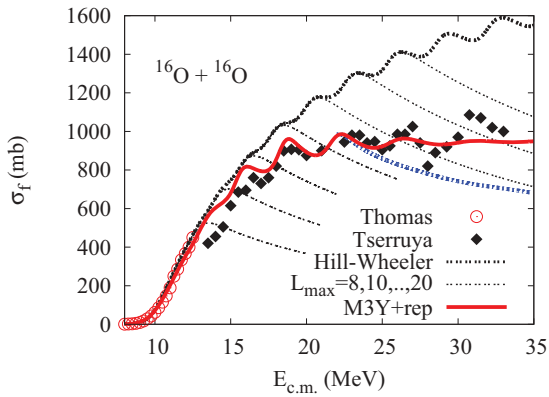

FIG. 4. (Color online) The measured fusion cross sections for $^{16}O + ^{16}O$ [4,14] are compared to the coupled-channels calculations (solid red curve) [7] that are based on the M3Y + repulsion potential. The thick (blue) dashed curve is the coupled-channels result for a maximum angular of $L_{max} = 16$. The thick, black dashed curve is the prediction of Hill-Wheeler's formula, whereas the thin dashed curves are the predictions for $L_{max} = 8, 10, \ldots, 20$.

At high energies it is often necessary to increase the values of the parameters W_0 and a_w if one wants to account for the data. This problem seems to be more serious for heavy systems where a large number of reaction channels that are not treated explicitly in the coupled-channels calculations open up. There are other aspects of the calculations that are questionable as the maximum angular momentum for fusion is reached. For example, angular momentum dissipation must play an important role at very high energies and the rotating frame approximation must therefore become questionable. These issues will not be addressed here.

A. Fusion of $^{16}O + ^{16}O$

The cross section one obtains by applying the Hill-Wheeler parametrization (2) to the fusion of $^{16}O + ^{16}O$ is compared in Fig. 4 to the high-energy data of Tserruya *et al.* [4] and also to the low-energy data of Thomas *et al.* [14]. The parameters are the same as used in the previous section. These parameters provide a fairly good description of the data at energies near the Coulomb barrier (and above 8 MeV) as illustrated in Fig. 1, but they fail to account for the high-energy data. One interpretation is that the centrifugal barriers predicted by Eq. (4) and the parameters considered here are not correct at high angular momenta.

The Hill-Wheeler cross sections one obtains for different choices of the maximum angular momentum for fusion, namely, $L_{max} = 8, 10, \ldots, 20$, are also shown in Fig. 4. They fall off as $1/E$ when the energy exceeds the height of the maximum barrier considered. To be specific, the cross section for a symmetric system behaves like

$$\sigma_f(E, L_{max}) \approx \frac{\pi\hbar^2}{2\mu E}\,[L_{max}(L_{max}+3)+2], \qquad (14)$$

when $E \gg V_B(L_{max})$. A similar expression holds for asymmetric systems with the L_{max} dependent factor replaced by $(L_{max}+1)^2$. The simple dependence on energy and maximum angular momentum is very useful because it can be used to roughly assign an angular momentum associated to each centrifugal barrier extracted from an experiment.

The fusion data shown in Fig. 4 follow the predicted $1/E$ dependence in small sections of energy but they do not agree with the magnitude of the curves predicted for different values of L_{max}. In fact, the data fall mostly halfway between these curves when the $1/E$ dependence occurs. This is a somewhat disturbing feature but it is nicely reproduced by the coupled-channels calculation of Ref. [7], which is shown by the solid (red) curve. The blue dashed curve shows the coupled-channels result one obtains by imposing a maximum angular momentum of $L_{max} = 16$. This curve does eventually approach the the Hill-Wheeler prediction for $L_{max} = 16$ but it occurs at an almost 10 MeV higher energy.

The coupled-channels calculation of Ref. [7] was calibrated to reproduce the low-energy fusion data of Thomas *et al.* [14]. It was supplemented with a short-ranged imaginary potential that acts near the minimum of the pocket in the entrance channel potential in order to improve the behavior at high energy. In spite of the latter adjustment, it is remarkable that the calculation does reproduce the high energy data so well up to about 27 MeV.

A good way to amplify the structures in the high energy data is to plot the first derivative of the energy weighted cross section. The result are shown in Fig. 5(a). The structures of the data are reproduced remarkably well in this representation by the coupled-channels calculation (the thick solid curve.) That gives confidence in the assignment of an angular momentum to each individual peak because the angular momenta of the calculated peaks are well determined. The peak associated with $L = 16$ is marked in the figure for clarity so that the peaks for $L = 12$ to 20 can easily be identified.

A similar coupled-channels calculation, which was based on a conventional Woods-Saxon potential, was also performed in Ref. [7]. It did a rather poor job in reproducing the data at high energy (see Fig. 7 of Ref. [7].) The barrier distributions one obtains from this calculation are shown in Fig. 5(b). While the location of the $L = 16$ peak is essentially the same as obtained with the M3Y + repulsion potential, the structures at smaller angular momenta have essentially disappeared. By comparing the two figures, Figs. 5(a) and 5(b), it is clear that the M3Y + repulsion potential provides the better description of the data.

B. Fusion of $^{12}C + ^{12}C$

Another example of a system that exhibits strong structures in its high-energy fusion data is $^{12}C + ^{12}C$ [1]. Unfortunately, it was not possible to reproduce the data so well by coupled-channels calculations, as it was done for the fusion of $^{16}O + ^{16}O$. It is therefore of interest to try a different approach when analyzing the data. One way is to use the Hill-Wheeler parametrization of the cross section, Eq. (2), and treat the energies of the centrifugal barriers, $V_B(L)$, as adjustable parameters.

The high-energy fusion data for $^{12}C + ^{12}C$ that were measured Sperr *et al.* [1] are shown in Fig. 6. Also shown is a prediction by Hill-Wheeler's formula, Eq. (2), which is based on the parameters: $V_{CB} = 6.23$ MeV, $\epsilon_0 = 0.4$ MeV,

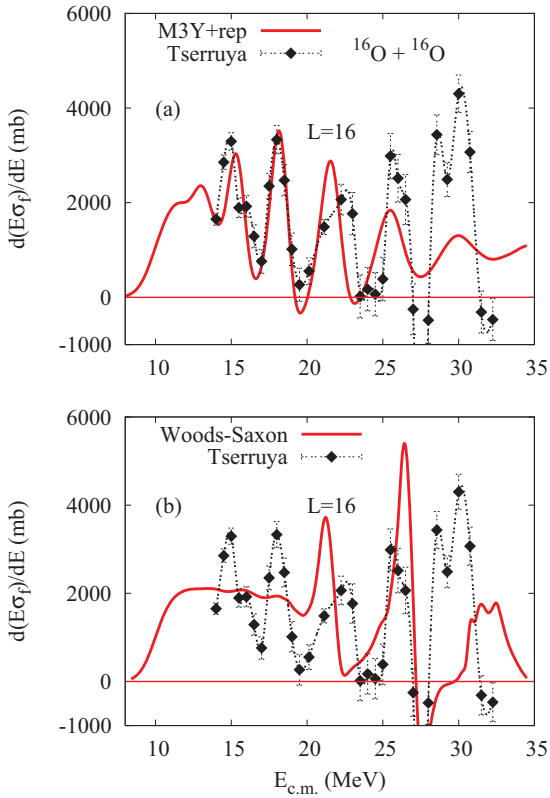

FIG. 5. (Color online) First derivative of the measured energy-weighted cross section for the fusion of $^{16}O + ^{16}O$ [4] is compared to coupled-channels calculations [7] that are based on the M3Y + repulsion potential (a), and on a conventional Woods-Saxon potential (b). The calculated peaks at $L = 16$ are marked.

and $R_{CB} = 7.667$ fm. These parameters characterize the entrance channel potential that was used in the coupled-channels calculations of Ref. [15]. The cross sections for different maximum angular momentum cutoffs, namely, for $L_{max} = 4$–16, are also shown. They coincide in most cases with the data when the data exhibit the characteristic $1/E$ dependence. One exception is at the highest energies, above 25 MeV, where the data fall half-way between the predictions for $L_{max} = 12$ and 14.

The fact that the data agree so well with the $1/E$ curves when the data exhibit the characteristic $1/E$ behavior, makes it fairly easy to fit the data simply by adjusting the heights of the centrifugal barriers. The result that gives the best fit to the data up to 25 MeV is shown by the solid curve in Fig. 6. A more detailed comparison is shown in Fig. 7 in terms of the first derivative of the energy-weighted cross section. Here one can see that the widths of the measured centrifugal barrier distributions apparently increase with increasing angular momentum, whereas the width was assumed to be a constant characterized by the parameter ϵ_0 in the calculation. It may be useful to incorporate an L dependence of the value of ϵ_L in the data analysis but that will not be tried here. The ultimate goal is to develop a coupled-channels description that can account for the data and provide a reliable determination of the angular momenta associated with the experimental peaks.

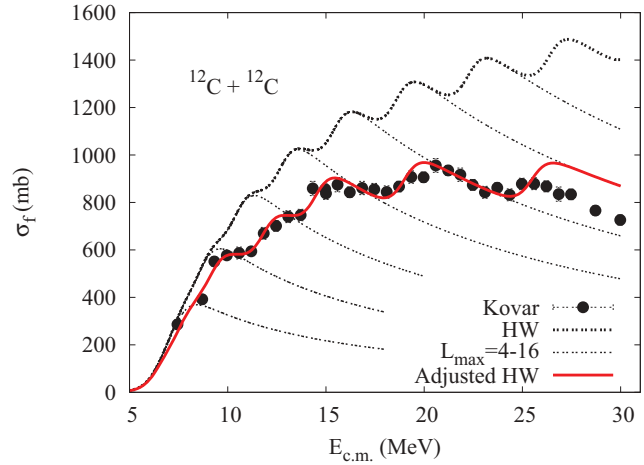

FIG. 6. (Color online) Cross sections for the fusion of $^{12}C + ^{12}C$ [1] are compared to the Hill-Wheeler expression (HW) using the parameters $V_{CB} = 6.23$ MeV, $R_{CB} = 7.667$ fm, and $\epsilon_0 = 0.4$ MeV. The solid curve was obtained by adjusting the heights of the centrifugal barriers to optimize the fit to the data below 25 MeV.

C. Fusion of $^{12}C + ^{16}O$

The last example in this section is the fusion of $^{12}C + ^{16}O$ which was also measured by Sperr *et al.* [2]. This is an asymmetric system so the fusion can occur for all values of L. The data are compared in Fig. 8 to coupled-channels calculations that include six channels (Ch6). The six channels are the elastic channel, the four channels associated with the excitation of the 2^+ and 3^- states in either projectile or target, and the channel associated with the excitation of the 0_2^+ in ^{12}C. The structure input to the calculation can be found in the papers on the fusion of oxygen plus oxygen [7] and carbon plus carbon [15].

The M3Y + repulsion, double-folding potential that is used in the calculation is generated from the charge densities of the reacting nuclei. The repulsive part of the interaction is determined by the incompressibility $K = 234$ MeV, and the diffuseness parameter a_r associated with the repulsion [11].

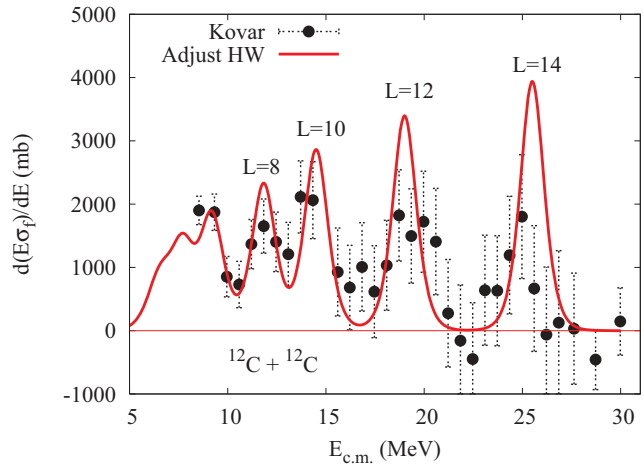

FIG. 7. (Color online) First derivative of the energy-weighted cross sections shown in Fig. 6.

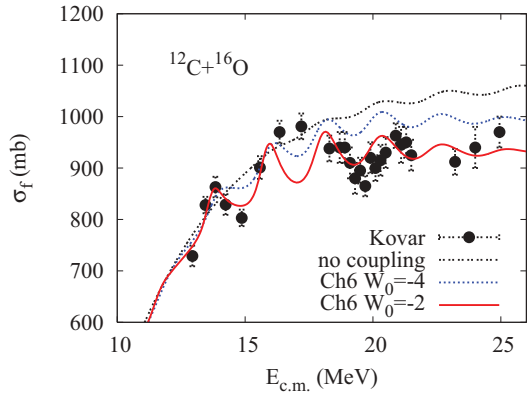

FIG. 8. (Color online) Cross sections for the fusion of $^{12}C + ^{16}O$ [2] are compared to coupled-channels calculations (Ch6) with different strengths of the imaginary potential ($W_0 = -2$ and -4 MeV, respectively), and to the no-coupling limit (top dashed curve).

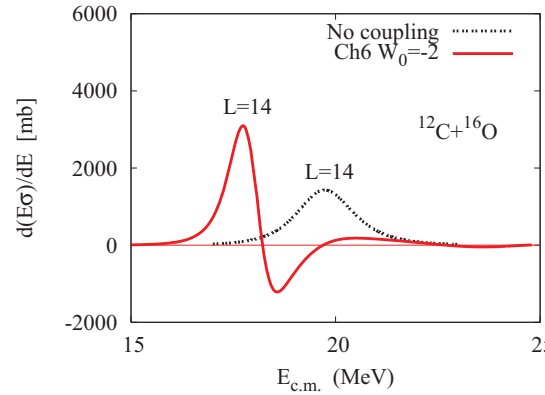

FIG. 10. (Color online) First derivative of the energy-weighted cross section obtained from the $L = 14$ partial wave. The peak of the coupled-channels calculation Ch6 is lowered by about 2 MeV compared to the peak obtained in the no-coupling limit.

The latter was set to $a_r = 0.41$ fm because that was the preferred value in the analysis [7] of the $^{16}O + ^{16}O$ fusion data by Thomas *et al.* [14].

The sensitivity to the imaginary potential is illustrated in Fig. 8 by two coupled-channels calculations, one with the strength $W_0 = -2$ MeV and one with $W_0 = -4$ MeV, whereas the diffuseness was kept fixed at $a_w = 0.2$ fm. It appears that the data are best described by the weaker absorption. The top dashed curve is the result of the no-coupling calculation which employs the weak absorption, $W_0 = -2$ MeV. Here the oscillations in the high energy cross sections are modest. Evidently, the strong structures in the solid curve of Fig. 8 are caused by coupled-channels effects.

The first derivative of the energy weighted cross sections is shown in Fig. 9. By comparing the data to the coupled-channels calculation (the one with the weak absorption, $W_0 = -2$ MeV) it is possible to assign an angular momentum to each of the observed peaks. Since the fusing systems is asymmetric, fusion occurs for both even and odd values of L. Calculated barriers

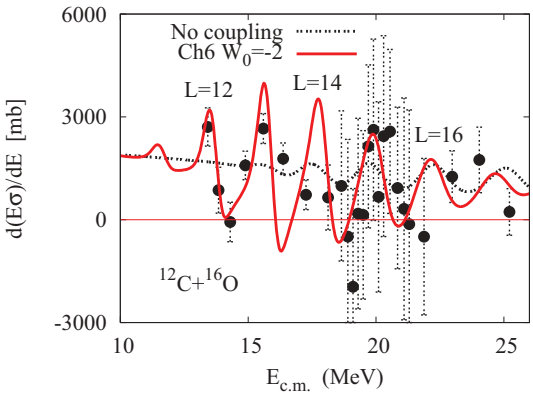

FIG. 9. (Color online) First derivative of some of the energy-weighted cross sections shown in Fig. 8. Both calculations include an imaginary potential with $W_0 = -2$ MeV. The peaks associated with $L = 12$, 14, and 16 in the Ch6 calculation are labeled.

exist for all values of angular momenta in the range $L = 11$–17, and the barriers for $L = 12$, 14, and 16 are marked for clarity in the figure. Experimental barriers are clearly identified for $L = 12$, 13, and 15 but the barrier for $L = 14$ is apparently missing.

It is remarkable that the Ch6 coupled-channels calculation shown in Fig. 9 reproduces the peak structures of the data so well, both in position and in absolute magnitude. The no-coupling limit, on the other hand, produces very modest peaks, and their positions are shifted compared to the peaks of the coupled-channels calculation. This is seen more clearly in Fig. 10, where the first derivative of the energy weighted contribution to the cross section from the orbital angular momentum $L = 14$ is shown. It is seen that the peak of the coupled-channels calculation is lowered by about 2 Mev compared to the no-coupling limit. This implies that the $L = 14$ peak obtained in the no-coupling limit is located in Fig. 9 near the $L = 15$ peak of the coupled-channels calculation.

In summary, structures due to individual centrifugal barriers are clearly observed in the fusion data for all three combinations of ^{12}C and ^{16}O nuclei. The coupled-channels calculations reproduce most of the observed structures fairly well, provided the M3Y + repulsion entrance channel potential is relatively shallow and the imaginary potential is relatively weak and short ranged. Using instead a conventional Woods-Saxon potential, the structures at low energies become suppressed, whereas the structures at higher energies become much stronger (see Fig. 5(b)). The results for $^{12}C + ^{16}O$ demonstrate that coupled-channels effects can be very large and shift the location of the effective centrifugal barrier to lower energies. The possibility of observing similar structures in the fusion of heavier systems is discussed in the next section.

IV. APPLICATIONS TO HEAVIER SYSTEMS

The search for structures in the high-energy fusion of heavier systems is difficult. The reason is that structures

associated with individual angular momentum barriers can only be seen at high angular momenta in heavy systems, according to Eqs. (10) and (11). Since many reaction channels are expected to open up at high angular momenta and high energies in heavy systems, the effect of couplings to these channels may smear out the peak structures. It is of great interest to pursue the search for such structures because they can provide valuable information (if they exist) about the ion-ion potential and put constraints on coupled-channels calculations. On the other hand, the disappearance of the structures may indicate where the coupling to many open reaction channels sets in.

An experimental search was performed by Gary and Volant [16] who investigated the fusion of $^{24}Mg + ^{24}Mg$, $^{28}Si + ^{28}Si$ and similar systems. The amplitudes of the oscillations that were observed are modest compared to the oscillations that are seen in the fusion of the ^{12}C and ^{16}O systems. They are sometimes comparable to the experimental uncertainties which makes it difficult to judge whether the structures exist or not. It was concluded [16] that $^{12}C + ^{24}Mg$ and $^{28}Si + ^{28}Si$ are the only systems that exhibit an oscillatory behavior in the fusion data at high energy. Although these findings are disappointing, it is useful to analyze the data the same way it was done in the previous section, namely, in terms of the first derivative of the energy weighted cross section. It is of particular interest to see whether the observed structures can be reproduced by coupled-channels calculations. As an example of a system that exhibits some structures, the fusion of the symmetric system $^{28}Si + ^{28}Si$ will be discussed in the following.

It is difficult to calibrate the M3Y + repulsion interaction to the $^{28}Si + ^{28}Si$ data by Gary and Volant [16] because they cover a relatively small range of energies. Fortunately, there is another data set by Nagashima *et al.* [17] which covers a much broader range of energies, and the high energy data by Vineyard *et al.* [18] are also very valuable because they determine a limiting or critical angular momentum for fusion, which is about $L_c = 38\hbar$. The three data sets are shown in Fig. 11. Also shown in this figure are coupled-channels calculations and calculations performed in the no-coupling limit. All calculations are based on an M3Y + repulsion potential, which is produced by ^{28}Si densities of radius $R = 3.17$ fm and diffuseness $a = 0.48$ fm. The diffuseness associated with the repulsive part of the interaction (see Ref. [11] for details) was adjusted to $a_r = 0.378$ fm so that the data by Nagashima *et al.* were reproduced (see below.)

The structure input to the calculations is shown in Table I. The calculations include the excitation of the 2^+ the 3^-, and an effective two-phonon quadrupole states in each nucleus. The two-phonon state was constructed following the procedure described in Ref. [20] from the information given in Table I about the 0_2^+ and 4^+ states. Unfortunately, there is no information available about the 2_2^+ state so it is ignored. The mutual $(2^+, 2^+)$, $(2^+, 3^-)$, and $(3^-, 2^+)$ excitations in projectile and target were also included, whereas the mutual excitation of the 3^- states was ignored because the excitation energy is so high. In addition to the elastic channel, that gives a total of $(1 + 3 + 3 + 3)$ ten channels and the calculation is referred to as the Ch10 calculation.

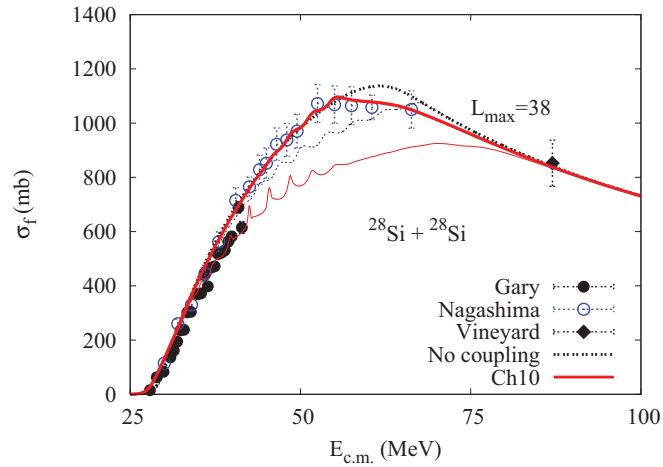

FIG. 11. (Color online) Measured cross sections for the fusion of $^{28}Si + ^{28}Si$ [16–18] are compared to coupled-channels calculations (Ch10, solid curves) and to calculations without couplings (dashed curves). The thin curves are based on a weak imaginary potential, with $a_w = 0.2$ fm, $W_0 = -2$ MeV, whereas the thick curves use a stronger imaginary potential, with $a_w = 0.5$ fm, $W_0 = -10$ MeV. All calculations assume a maximum angular momentum of $L_{max} = 38$.

The nucleus ^{28}Si is deformed with an oblate quadrupole shape. The measured quadrupole moment of the 2^+ state, $Q_2 = 0.16(3)$ b [21], implies a deformation parameter which is $\beta_2 = -0.40(8)$. This is consistent with the measured $B(E2)$ value given in Table I. The quadrupole deformation was considered explicitly in the coupled-channels calculations by including the diagonal matrix element of the quadrupole interaction in the excited 2^+ state (see Ref. [20] for details.)

It is difficult to make a good calibration of the M3Y + repulsion interaction without access to any data at sub-barrier energies. The cross sections at high energies are sensitive to other reaction mechanisms that are not considered explicitly in coupled-channels calculations, so there is some ambiguity in the calibration of the ion-ion potential and the imaginary potential. The thick solid curve in Fig. 11 is a compromise which does a fairly good job in reproducing the data of Nagashima *et al.* [17]. It is based on a relatively strong imaginary potential, $W_0 = -10$ MeV and $a_w = 0.5$ fm. Moreover, a maximum angular momentum for fusion, $L_{max} = 38$,

TABLE I. The properties of the low-lying states in ^{28}Si are from Ref. [19]. The 0_2^+ and 4^+ states are lumped together into one effective two-phonon quadrupole state as described in Ref. [20]. Unfortunately, no information about the 2_2^+ state is available. The Coulomb and nuclear deformation parameters are assumed to be the same.

I^π	E_x (MeV)	Transition	$B(E\lambda)$ (W.u.)	β_λ^C
2_1^+	1.779	$2_1^+ - 0_1^+$	13.2(3)	−0.411
0_2^+	4.980	$0_2^+ - 2_1^+$	8.6(16)	
4^+	4.618	$4^+ - 2_1$	13.8(13)	
Eff 2PH	4.689	$2PH - 2_1^+$	8.8	−0.238
3^-	6.879	$3^- - 0_1^+$	13.9(24)	0.416(35)

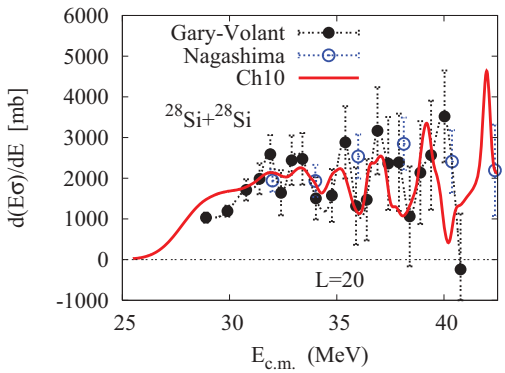

FIG. 12. (Color online) First derivative of the energy-weighted cross sections shown in Fig. 11. The coupled-channels calculation Ch10 is based on the weak imaginary potential, with $a_w = 0.2$ fm, $W_0 = -2$ MeV. The calculated peak for $L = 20$ near 35 MeV is indicated.

was imposed on the calculations in order to be consistent with the high energy data of Vineyard *et al.* [18]. The thin solid curve is the result of a similar calculation that is based on a weaker and short-ranged imaginary potential, $W_0 = -2$ MeV and $a_w = 0.2$ fm. It does not account for Nagashima's data at high energies but it is in fair agreement with the data by Gary and Volant.

The first derivative of the energy-weighted cross section for the fusion of $^{28}\mathrm{Si} + ^{28}\mathrm{Si}$ is shown in Fig. 12. The data by Gary and Volant [16] are connected by the dashed curve for clarity. The data by Nagashima *et al.* [17] are also shown. They are consistent with the data by Gary and Volant but the energy steps between the data points are too large to reveal any structures in the data.

The solid curve in Fig. 12 is derived from the coupled-channels calculation shown in Fig. 11 with the weak absorption. It shows a lot of structure and it is remarkable how well the peaks of the calculation correlate with the structures observed in the data. The good agreement in this respect allows one to assign with some confidence an angular momentum to each of the peaks. The peak near 35 MeV is caused by the $L = 20$ centrifugal barrier.

Based on the results discussed here it is suggested that some of the measurements by Gary and Volant [16] should be repeated with higher precision and with sufficiently small energy steps so that the structures associated with the individual centrifugal barriers can better be resolved. In order to be able to calibrate the ion-ion potential, it would be very useful not only to perform the measurements at energies above the Coulomb barrier, where the structures due to the individual centrifugal barriers may exist, but also at energies far below the Coulomb barrier, where the sensitivity to the ion-ion potential for overlapping nuclei also shows up [11].

The analysis of the ^{28}Si fusion data shows that it is necessary to employ an imaginary potential of varying strength, depending on which data set is analyzed. The high-energy data require a strong imaginary potential, combined with a maximum angular momentum for fusion, whereas the low energy data can be explained with a weak imaginary potential. It would be useful in future work to develop an energy dependent imaginary potential.

V. CONCLUSIONS

The structures that have been observed a long time ago in the high-energy data for several light-ion systems can be explained as being caused by the penetration of successive centrifugal barriers that are well separated in energy. This mechanism is clearly seen in Hill-Wheeler's expression for the fusion cross section, and it is best illustrated by plotting the first derivative of the energy weighted cross section. The locations of the peaks in such a plot show the energies of the centrifugal barriers that causes the structures, whereas the width of the peaks can be associated with the quantum mechanical penetration of the centrifugal barrier. The analytic expression for the fusion cross section derived by Wong, on the other hand, does not reveal the energy location of any individual centrifugal barriers, except the location of the s-wave barrier. This is not surprising because the derivation of Wong's formula assumes that sequential barriers are so close in energy that the discrete sum over the orbital angular momentum be replaced by a smooth integration.

Some of the fusion data were analyzed by coupled-channels calculations that were based on the M3Y + repulsion potential. The calculations showed that the strength and the location of the peaks observed in the first derivative of the energy-weighted cross section are very sensitive to coupled-channels effects. This implies that the extracted barriers are effective barriers and not the real barriers of the centrifugal potential in the entrance channel.

The nuclear potentials that were used in the coupled-channels calculations were adjusted in each case to optimize the fit to the data, and when this was achieved, it turned out that the calculations reproduced fairly well the location of the peak structures that are observed in the data. The good agreement allows one to assign an orbital angular momentum to most of the effective centrifugal barriers that have been extracted from the experiments.

The results of the data analysis suggest that the structures observed in the fusion data at energies above the Coulomb barrier are best explained by coupled-channels calculations that are based on a shallow potential in the entrance channel. Thus there appears to be some consistency in the description of the structures at energies above the Coulomb barrier and the hindrance of fusion, which is observed at energies far below the Coulomb barrier. Both phenomena are sensitive to the ion-ion potential for overlapping nuclei, and both are best described by a shallow potential in the entrance channel.

The amplitude of the structures observed in the fusion data seems to diminish in heavier systems. This is unfortunate because the structures reveal valuable information about the ion-ion potential, and they provide an excellent test of coupled-channels calculations. It is very encouraging to see, however, that structures do exist in the fusion of a system as heavy as $^{28}\mathrm{Si} + ^{28}\mathrm{Si}$. It is therefore suggested that a new experimental search for structures in high-energy fusion

cross sections be pursued, preferably with higher precision than in the past, and with energy steps that are sufficiently small to resolve the structures associated with the individual barriers.

ACKNOWLEDGMENTS

This work was supported by the US Department of Energy, Office of Nuclear Physics, contract no. DE-AC02-06CH11357.

[1] P. Sperr, T. H. Braid, Y. Eisen, D. G. Kovar, F. W. Prosser Jr., J. P. Schiffer, S. L. Tabor, and S. E. Vigdor, Phys. Rev. Lett. **37**, 321 (1976); see also Ref. [3].
[2] P. Sperr, S. E. Vigdor, Y. Eisen, W. Henning, D. G. Kovar, T. R. Ophel, and B. Zeidman, Phys. Rev. Lett. **36**, 405 (1976); see also Ref. [3].
[3] D. G. Kovar *et al.*, Phys. Rev. C **20**, 1305 (1979).
[4] I. Tserruya, Y. Eisen, D. Pelte, A. Gavron, H. Oeschler, D. Berndt, and H. L. Harney, Phys. Rev. C **18**, 1688 (1978).
[5] J. J. Kolata, R. C. Fuller, R. M. Freeman, F. Haas, B. Heusch, and A. Gallmann, Phys. Rev. C **16**, 891 (1977).
[6] R. Vandenbosch, Phys. Lett. B **87**, 183 (1979).
[7] H. Esbensen, Phys. Rev. C **77**, 054608 (2008).
[8] D. L. Hill and J. A. Wheeler, Phys. Rev. **89**, 1102 (1953).
[9] C. L. Jiang *et al.*, Phys. Rev. Lett. **89**, 052701 (2002).
[10] C. L. Jiang, B. B. Back, H. Esbensen, R. V. F. Janssens, and K. E. Rehm, Phys. Rev. C **73**, 014613 (2006).
[11] Ş. Mişicu and H. Esbensen, Phys. Rev. C **75**, 034606 (2007).
[12] C. Y. Wong, Phys. Rev. Lett. **31**, 766 (1973).
[13] N. Rowley, G. R. Satchler, and P. H. Stelson, Phys. Lett. B **254**, 25 (1991).
[14] J. Thomas, Y. T. Chen, S. Hinds, D. Meredith, and M. Olson, Phys. Rev. C **33**, 1679 (1986).
[15] H. Esbensen, X. Tang, and C. L. Jiang, Phys. Rev. C **84**, 064613 (2011).
[16] S. Gary and C. Volant, Phys. Rev. C **25**, 1877 (1982).
[17] Y. Nagashima *et al.*, Phys. Rev. C **33**, 176 (1986).
[18] M. F. Vineyard *et al.*, Phys. Rev. C **41**, 1005 (1990).
[19] Evaluated Nuclear Data Structure Files, Nuclear Data Center, Brookhaven National Laboratory [http://www.nndc.bnl.gov].
[20] H. Esbensen, Phys. Rev. C **68**, 034604 (2003).
[21] N. J. Stone, At. Data Nucl. Data Tables **90**, 75 (2003).